Ethane/Ethylene Adsorption on Carbon Nanotubes: Temperature and Size Effects on Separation Capacity

Alberto G. Albesa,*,[†] Matías Rafti,[†] Dinesh S. Rawat,[‡] José Luis Vicente,[†] and Aldo D. Migone[‡]

[†]Instituto de Investigaciones Fisicoquímicas Teóricas y Aplicadas (INIFTA), Departamento de Química, Facultad de Ciencias Exactas, Universidad Nacional de La Plata (UNLP), CC 16, Sucursal 4 (1900) La Plata, Argentina

[‡]Department of Physics, Southern Illinois University, Carbondale, Illinois 62901, United States

ABSTRACT: We present the results of Monte Carlo simulations of the adsorption of single-component ethane and ethylene and of equimolar mixtures of these two gases on bundles of closed, single-walled carbon nanotubes. Two types of nanotube bundles were used in the simulations: homogeneous (i.e., those in which all the nanotubes have identical diameters) and heterogeneous (those in which nanotubes of different diameters are allowed). We found that at the same pressure and temperature more ethane than ethylene adsorbs on the bundles over the entire range of pressures and temperatures explored. The simulation results for the equimolar mixtures show that the pressure at which maximum separation is attained is a very sensitive function of the diameter of the nanotubes present in the bundles. Simulations using heterogeneous bundles yield better agreement with single-component experimental data for isotherms and isosteric heats than those obtained from simulations using homogeneous bundles. Possible applications of nanotubes in gas separation are discussed. We explored the effect of the diameter of the nanotubes on the separation ability of these sorbents, both for the internal and for the external sites. We found that substrate selectivity is a decreasing function of temperature.
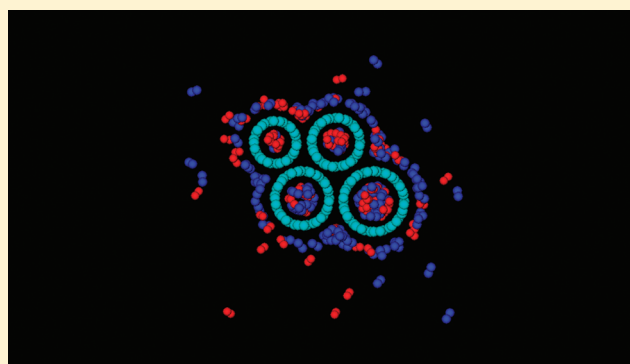
INTRODUCTION

Olefin/paraffin separations are among the most important processes in the chemical and petrochemical industries. The production of plastics, rubber, films, and other chemicals requires the use of high-purity ethylene (>99.9%). Ethylene is normally produced by "cracking", i.e., the thermal decomposition of ethane. This process produces an ethane/ethylene mixture that has to be separated to produce high-purity ethylene. Cryogenic distillation remains the dominant technology for ethane/ethylene separation. Unfortunately, cryogenic distillation has high levels of energy consumption and high equipment costs associated with it. In a typical ethylene-producing plant, cracking equipment represents approximately 25% of the total cost, while the remainder of the cost is due to the compression, heating, dehydration, recovery, and refrigeration equipment.[1]

Alternative methods for olefin/paraffin separation that do not require cryodistillation would reduce a plant's energy and equipment costs. Consequently, the search for alternative separation techniques has generated much interest. Some of the new separation techniques being explored include[2] extractive distillation, chemical and physical adsorption, and resin-based membrane separation.[3]

Adsorption-based gas mixture separation methods are one of the approaches under active investigation. Sorbent materials used for paraffin/olefin separation typically incorporate transition metals in them (e.g., Cu, Ag). The presence of these metals results in the preferential adsorption of the olefin because of the strong interaction between the olefin's unsaturated bonds and the metal ions on the sorbent, which result in π-complexation. Preferential adsorption of the olefin[4] results in a process that purifies the paraffin. Conversely, the availability of materials that result in the preferential adsorption of the paraffin would provide the basis for a suitable alternative process for olefin purification and separation. Unfortunately, very few materials have been found that belong in this group (recently it has been shown[5] that aluminum methylphosphonate polymorph alpha (AlMePO-α) preferentially adsorbs paraffins as a result of the interaction between the methyl groups in the adsorbent and those in the adsorbate[6]).

Experimental data on gas mixture adsorption are scarce. As a result, the analysis of equilibrium properties of multicomponent adsorbed systems is rather heavily reliant on empirical and theoretical models that allow one to estimate multiple-component equilibrium properties from single-component data.

In the case of carbon nanotube substrates, few experimental reports are available even for single-component gas adsorption of ethane[7] or ethylene.[8] The reports that are available describe measurements performed at cryogenic temperatures[7,8] (which do not provide the information needed for room temperature applications).

Some theoretical work has been reported for linear hydrocarbon adsorption on single-walled carbon nanotube (SWNT)

bundles. Jiang et al.[9] explored the adsorption and separation of linear and branched alkanes (between one and five C atoms) on bundles through configurational-bias Monte Carlo simulations at 300 K. Because they used the bundle as a periodic hexagonal arrangement, only adsorption at the interior sites was considered, and on the interstitial sites when these were simulated to be large enough to allow for adsorption on them. In essence what was modeled was an infinitely wide bundle, where no surface effects were considered. This study observed that for multi-component alkane mixtures at low pressures the longer molecules are favored; as the pressure is increased, the longer alkanes are replaced by the shorter ones as a result of the size entropy effect. Cruz et al.[10] studied the thermodynamics of alkanes and alkenes adsorbed on homogeneous SWNT bundles at room temperature through configurational-bias grand canonical Monte Carlo simulations. In this study, all four groups of adsorption sites on the bundles (grooves, outer surface sites, interior sites, and interstitial sites) (see Scheme 1) were considered. These

Scheme 1. Types of Adsorption Sites: Grooves between Two Tubes (G Sites), on the Surface of the Nanotube (S Site), in the Interior of the Same (T Sites) in the Case of Opened Tubes, and in Interstitial Channels (IC Sites)
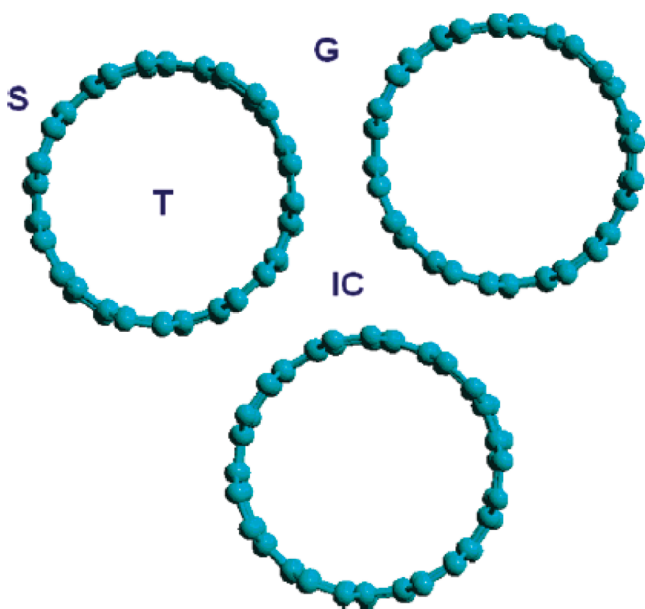
theoretical studies determined the adsorption isotherms and the isosteric heats of adsorption, q_{st}, for these systems for homogeneous bundles of nanotubes and showed how these quantities changed with the nanotube diameter.

Experimental data (from temperature-programmed desorption experiments) are available. These studies investigated the desorption of longer alkanes, pentane to nonane, from bundles of chemically opened single-walled carbon nanotubes. These experiments found clearly distinguishable desorption peaks associated with each one of the four groups of adsorption sites present in the bundles.[11]

Single-component adsorption experiments on carbonaceous sorbents have found that, under the same conditions, ethane is adsorbed in greater amounts than ethylene over a wide range of temperatures and pressures.[12] Carbon nanotubes, thus, are a promising sorbent on which to explore olefin/paraffin separation.

Here we present the results of a computer simulation study of the adsorption of ethane, ethylene. and equimolar mixtures of these two gases on homogeneous and heterogeneous bundles of SWNTs. Homogeneous bundles consist of nanotubes of identical diameter packed on triangular arrays, while heterogeneous bundles are modeled using nanotubes of different diameters, with a diameter distribution selected to reflect the experimental results.[13−16] We have explored how temperature and nanotube diameter affect the selectivity of these sorbents by performing simulations below, near, and above the critical point on bundles composed of nanotubes with radii between 11 and 18 Å.

■ SUBSTRATE MODELS USED AND SIMULATION DETAILS

In previous work we performed simulations on homogeneous bundles[17] using the simplest bundle that had all four types of sites present (namely, grooves, outer sites, internal sites, and interstitial channels). We used a triangular array of just three individual nanotubes. Here we extend this approach to heterogeneous nanotube bundles.

Three different triangular arrays were used to model homogeneous nanotube bundles. The nanotube diameters considered were 9.49, 13.60, and 20.34 Å corresponding to (7,7), (10,10), and (12,12) nanotubes, respectively, where (n,n) represent the Hamada index. The distance between the tubes was fixed at 3.4 Å in all cases.

Recently, LaBrosse et al.[14,16] have shown that the best agreement between adsorption experiments and simulations is attained when the bundles of SWNTs are modeled as being heterogeneous. To implement this approach, we have used three heterogeneous bundle models to reproduce the diameter distributions found experimentally, specifically (1) NT_Mix1, consisting of one (7,7) nanotube, four (10,10) nanotubes, and one (12,12) nanotube, (2) NT_Mix2, consisting of one (7,7) nanotube, one (8,8) nanotube, one (9,9) nanotube, and one (10,10) nanotube, and (3) NT_Mix3, consisting of one (10,10)
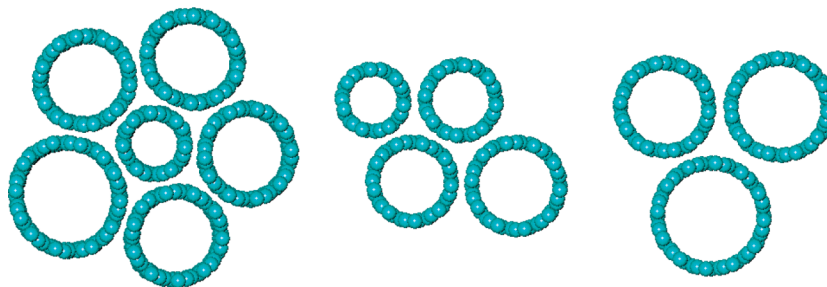

Figure 1. Heterogeneous nanotube clusters employed in the simulations. Sizes from left to right are NT_Mix1, NT_Mix2, and NT_Mix3, respectively.

nanotube, one (11,11) nanotube, and one (12,12) nanotube. They are shown in Figure 1.

Interaction between molecules was modeled via a 12−6 Lennard-Jones potential. We considered the AU-TraPPE model for ethylene and ethane, with the molecular parameters proposed by Martin and Siepmann[18] for ethane and those proposed by Wick et al.[19] for ethylene. This approach replaces a C atom and the H atoms bonded to it in a hydrocarbon molecule by a single "pseudoatom" (e.g., CH_4, CH_3, CH_2, and CH). This reduces the number of interacting sites by about one-third and results in a computational time that is shorter by approximately 1 order of magnitude.

The TraPPE force field provides a good description for alkanes and alkenes. This force field is built around the following parameters: (1) a C−C bond length for the alkanes and a different bond length for the alkenes, (2) a C−C−C bond angle for the alkanes and a different one for the alkenes, and (3) a dihedral potential common for alkanes and alkenes.

Table 1 presents the values of the force field parameters used for selected pseudoatoms included in the simulations.

Table 1. Pseudoatom Potentials According to the AU-TraPPE Model

pseudoatom	ε (K)	σ (Å)
CH_3 (sp^3)	98	3.75
CH_2 (sp^2)	85	3.675

In principle, one can consider taking into account a larger set of pseudoatoms. However, such an approach would require the use of a large number of parameters, so we opted to sacrifice somewhat the precision of our calculations to gain simplicity. The parameters used in all the Monte Carlo simulations presented in this work are as follows: (1) The length of the side of the simulation box was 10σ. (2) The cutoff radius was 4σ. (3) A total of 2.5×10^6 Monte Carlo steps were used for thermalization (including creation, destruction, or displacement attempts for each molecule); these were followed by 5×10^4 steps for determining the statistical averages. (4) Owing to the cutoff radius chosen, long-distance corrections were not performed.

■ ISOSTERIC HEAT OF ADSORPTION

The isosteric heat of adsorption for the ith component of an ideal gas mixture, $q_{st,i}$, can be calculated using the following expression:

$$\frac{q_{st,i}}{RT^2} = \left[\frac{d \ln p_i}{dT}\right]_{n_i} \quad (1)$$

where $p_i = Py_i$ stands for the partial pressure of the ith component (P and y_i are the total gas pressure and molar fraction in the gas phase) in equilibrium with n_i moles in the adsorbed phase, T is the temperature, and R is the gas constant.[20] Equation 1 is not a practical method for calculating the isosteric heat because the data required for using eq 1 are rarely found in the literature.[21]

In Monte Carlo simulations, the isosteric heat can be calculated from the following equation:

$$q_{st,i} = (H^b - H^{*,b}) + RT - \left(\frac{\partial U^{a,c}}{\partial N^a}\right)_{T,V^a} \quad (2)$$

where the superscripts a and b and * respectively denote the values of the thermodynamic functions for the adsorbed, gas, and ideal phases. $U^{a,c}$ is the configurational part of the interaction

energy, which includes both adsorbate−adsorbate and adsorbate−adsorbent interactions. Assuming that the gas behaves as an ideal gas, eq 2 becomes

$$q_{st,i} = RT - \left(\frac{\partial U^{a,c}}{\partial N^a}\right)_{T,V^a} \quad (3)$$

Here $\partial U^{a,c}/\partial N$ can be obtained either by numerical differentiation or from fluctuation theory:

$$\left(\frac{\partial U^{a,c}}{\partial N^a}\right) = \frac{f(U, N)}{f(N, N)} \quad \text{where} \quad f(X, Y) = \langle XY \rangle - \langle X \rangle \langle Y \rangle \quad (4)$$

Here the angular brackets indicate the mean value of the quantity.

The heat of adsorption of the ith component of a binary mixture can be obtained from the simulations solving the following expressions:

$$q_{st,i} = RT - \left(\frac{\partial U^{a,c}}{\partial N_i^a}\right)_{T,V^a,N_{j\neq i}^a} \quad (5)$$

$$\left(\frac{\partial U^{a,c}}{\partial N^a}\right) = \sum_k \left(\frac{\partial U^{a,c}}{\partial \beta \mu_k}\right)_{T,V^a,N_{j\neq i}^a} \left(\frac{\partial \beta \mu_k}{\partial N_i^a}\right)_{T,V^a,N_{j\neq i}^a} \quad (6)$$

where

$$\left(\frac{\partial U^{a,c}}{\partial \beta \mu_k}\right)_{T,V^a,N_{j\neq i}^a} = f(U, N_k^a) \quad (7)$$

$$\begin{pmatrix} \dfrac{\partial \beta \mu_1}{\partial U_1^a} & \dfrac{\partial \beta \mu_1}{\partial U_2^a} \\ \dfrac{\partial \beta \mu_2}{\partial U_1^a} & \dfrac{\partial \beta \mu_2}{\partial U_2^a} \end{pmatrix} = \begin{pmatrix} f(N_1^a, N_1^a) & f(N_1^a, N_2^a) \\ f(N_2^a, N_1^a) & f(N_2^a, N_2^a) \end{pmatrix}^{-1} \quad (8)$$

The isosteric heat of adsorption of the components of a gas mixture is a useful quantity for understanding a sorbent's selectivity. The selectivity $S_{i,j}$ of the ith species relative to the jth species can be defined as follows:

$$S_{i,j} = \frac{\theta_i/\theta_j}{p_i/p_j} \quad (9)$$

Here θ_i and θ_j are the sorbent loadings for species i and j and p_i and p_j the corresponding partial pressures.

■ RESULTS

Single-Component Adsorption. *Homogeneous Nanotubes.* *(7,7) Nanotubes.* Figure 2 shows adsorption isotherms calculated at $T = 153$, 273, and 343 K for ethane and ethylene on homogeneous (7,7) nanotube bundles. The initial adsorption, which occurs on the sites at the interior of the nanotubes, starts at very low pressures. For both ethane and ethylene, the data corresponding to the 153 K isotherm display a substep near $\langle N \rangle = 220$, with $\langle N \rangle$ being the average number of adsorbed molecules. This feature can be attributed to the completion of the first layer on the external surface of the bundle. At 153 K the results for ethane and ethylene are quite similar for the high pressure regime, while some differences between the gases exist at low pressures. The effect of increasing
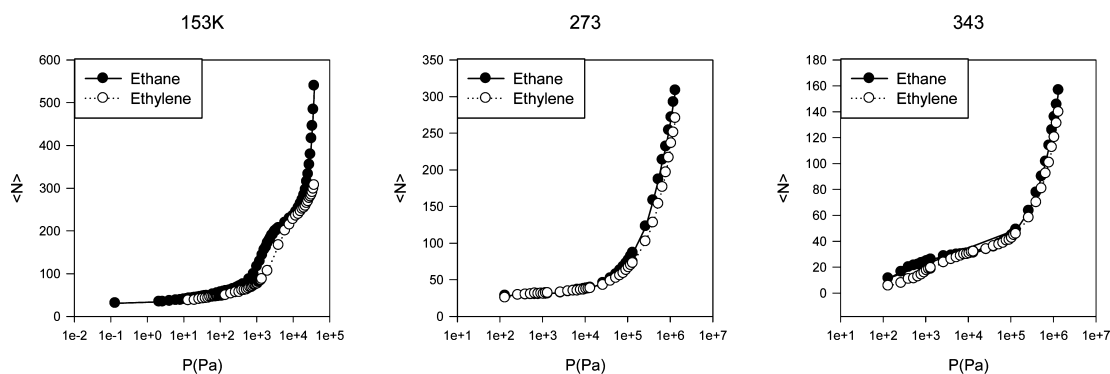
Figure 2. Simulated adsorption isotherms at 153, 273, and 343 for ethane (filled circles) and ethylene (open circles) for (7,7) homogeneous nanotube bundles.
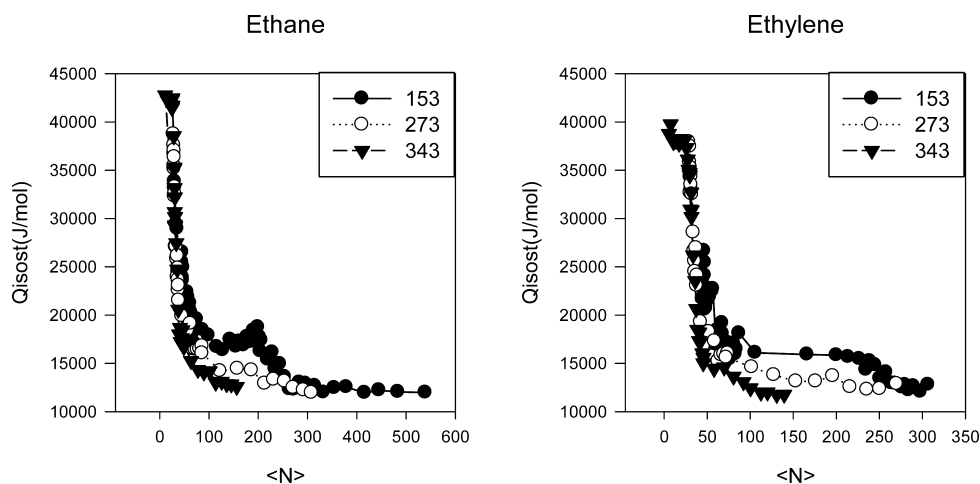

Figure 3. Isosteric heat of adsorption obtained from the simulations for ethane (left) and ethylene (right) at 153 K (filled circles), 273 K (open circles), and 343 K (inverted filled triangles) for (7,7) homogeneous nanotube bundles, with $\langle N \rangle$ being the average number of adsorbed molecules.
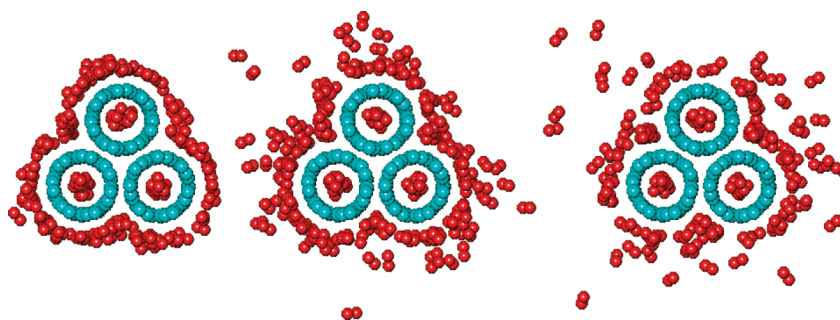

Figure 4. Upper view snapshots of adsorbed molecules on (7,7) homogeneous nanotube bundles at different temperatures. The temperatures, from left to right, are 153, 273, and 343 K, respectively, and the number of adsorbed molecules is the same in all cases.

temperature is to reduce the differences between the simulated isotherms for these two species.

The sequential filling of the adsorption sites is also reflected in the isosteric heat profiles shown in Figure 3. The q_{st} profile for ethane at T = 153 K exhibits a peak near $\langle N \rangle$ = 200 which is not present at higher temperatures. This feature resembles experimental data found in the literature for ethane on strongly graphitized surfaces at monolayer completion[20] (which on the outside of the bundle should occur at $\langle N \rangle$ = 200).

Figure 4 shows simulation snapshots at different temperatures with the same number of molecules in the simulation box. Disorder at the outer surface of the bundle increases with temperature as expected.

(10,10) Nanotubes. The isotherms simulated using (10,10) nanotube bundles exhibit a substep at $\langle N \rangle$ = 100 as can be seen in Figure 5. For the 153 K isotherms, this substep occurs at a pressure that is about 4 orders of magnitude lower than that corresponding to the monolayer completion on the external sites seen in the (7,7) bundles at the same temperature. This feature near $\langle N \rangle$ = 100 can be attributed to the filling of the internal sites on these nanotubes.

For both ethane and ethylene at T = 153 K (as was the case for the (7,7) nanotubes) there is another substep corresponding to monolayer completion on the external surface of the bundles. In this case, monolayer completion occurs near $\langle N \rangle$ = 350.
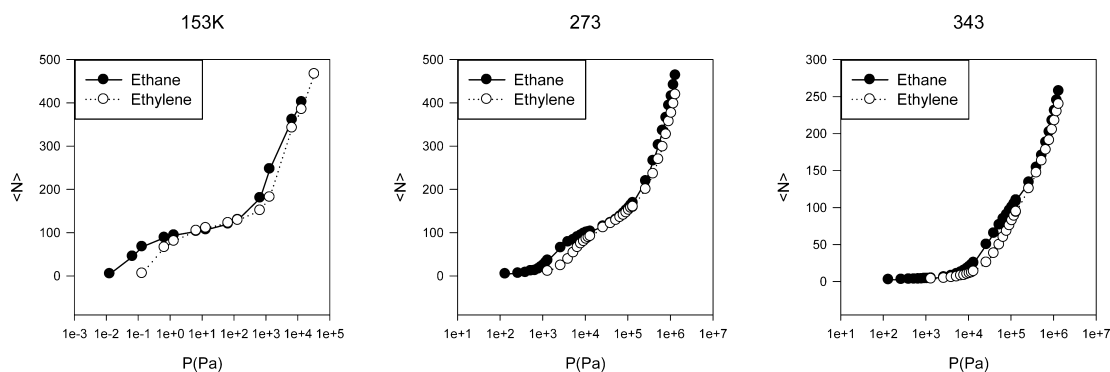
Figure 5. Simulated adsorption isotherms at 153, 273, and 343 K for ethane (filled circles) and ethylene (open circles) for (10,10) homogeneous nanotube bundles.
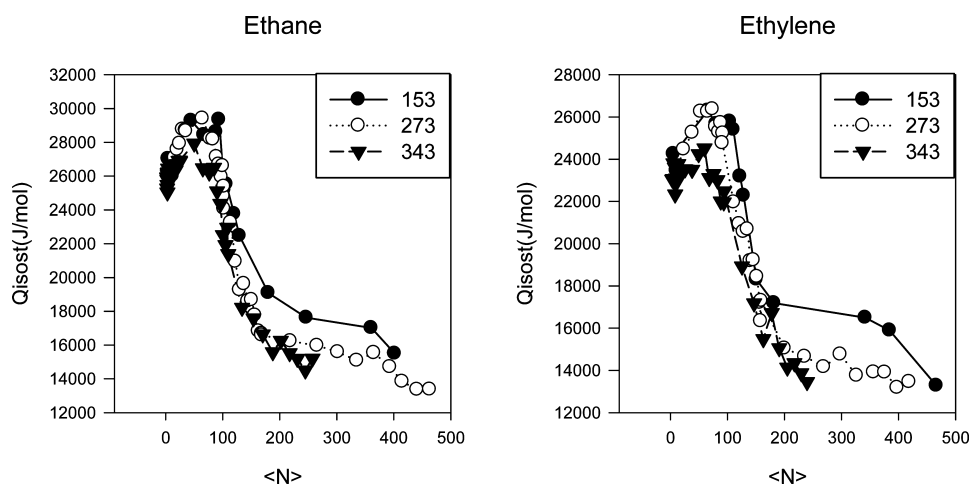

Figure 6. Isoteric heat of adsorption obtained from the simulations for ethane (left) and ethylene (right) at 153 K (filled circles), 273 K (open circles), and 343 K (inverted filled triangles) for (10,10) homogeneous nanotube bundles, with $\langle N \rangle$ being the average number of adsorbed molecules.

Figure 6 shows the calculated isosteric heats of adsorption as a function of the sorbent loading corresponding to the three temperatures studied. Interestingly, for ethane, the isosteric heat value corresponding to the interior sites is independent of temperature. This is not the case for the q_{st} values corresponding to adsorption on sites on the external nanotube surface, which decrease slightly as the temperature is increased. The observed temperature independence results from the fact that the density of the adsorbed phase in the interior sites of these nanotubes remains constant for all three temperatures, while this is not the case on the external sites.

(12,12) Nanotubes. The adsorption isotherms and the isosteric heats calculated for the (12,12) nanotubes show the same trends observed for (10,10) nanotubes. Namely, there is a first substep corresponding to the monolayer completion on the inner sites (now occurring near $\langle N \rangle$ = 150) and a second substep corresponding to monolayer completion on the external sites (now near $\langle N \rangle$ = 420); the latter substep is resolvable only at the lowest temperature.

The isosteric heat profiles for the (12,12) nanotubes, not shown in the figures, only differ from those for the (10,10) nanotubes in that the value of the isosteric heat for the interior sites now is seen to decrease with increasing temperature. This decrease is a reflection that for these nanotubes the loading of the interior sites decreases with increasing temperature. As was the case with the other tubes, an isosteric heat peak is also

present at the completion of the monolayer on the external sites for the lowest temperature.

Heterogeneous Nanotubes. Figure 7 presents the isosteric heats q_{st} obtained for single-component ethane and ethylene films adsorbed on the heterogeneous bundle we labeled NT_Mix1. The very high values of the isosteric heat at low $\langle N \rangle$ correspond to the filling of the internal sites of the (7,7) nanotubes. The isosteric heat peak present near $\langle N \rangle$ = 70 corresponds to the filling of the interior sites of the (10,10) nanotube.

The adsorption capacities for ethane and ethylene on the NT_Mix2 heterogeneous bundle show similar behaviors for the entire pressure and temperature ranges explored, as was the case with these two adsorbates on the (7,7) homogeneous bundles. Unlike what occurs with homogeneous bundles, the isosteric heats do not present any peaks or sharp features. Rather, they just show a steep decrease.

Density profiles for $\langle N \rangle$ = 250, presented in Figure 8, show that all the tubes are filled and that the external monolayer is complete. One can observe a region of surprisingly lower loading on the outer sites of the (7,7) nanotube (the leftmost nanotube in this figure). This reflects the fact that, due to the strong curvature of this small-diameter nanotube, the interaction between ethylene molecules is weaker.[22]

The results obtained for the isosteric heat profiles on the NT_Mix3 heterogeneous bundle, not shown in the figures,
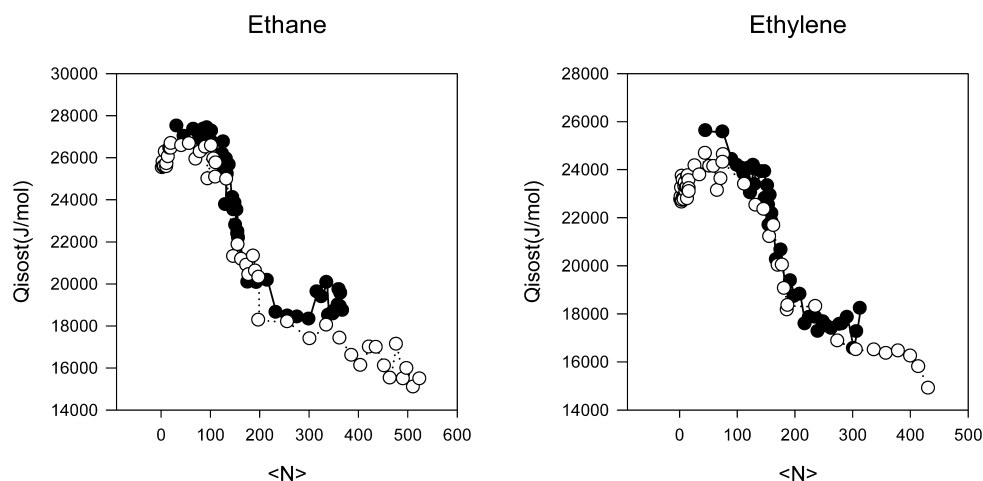
Figure 7. Isosteric heat of adsorption obtained from the simulations for ethane (left) and ethylene (right) at 153 K (filled circles), 273 K (open circles), and 343 K (filled triangles) for NT_Mix3 heterogeneous nanotube bundles, with $\langle N \rangle$ being the average number of adsorbed molecules.
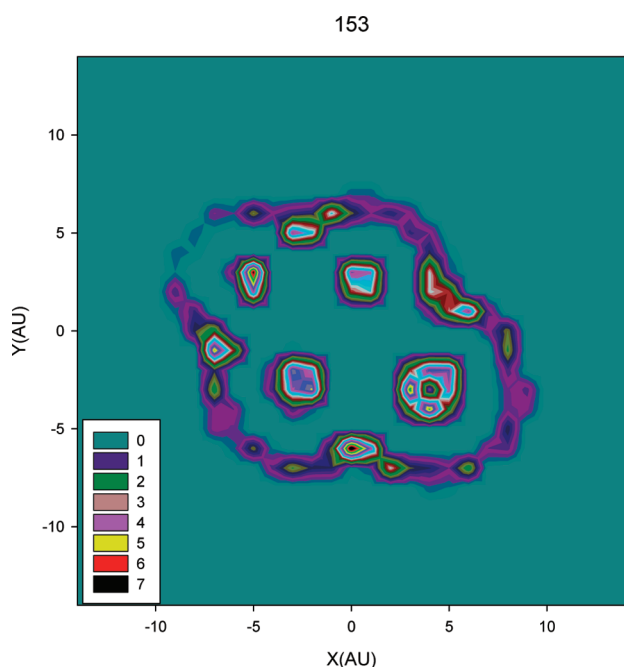

Figure 8. Density 2D profiles at high coverage and 153 K for ethylene in Nt_Mix2. The color scale is inset and represents the average number of molecules.

Figure 9. Comparison of experimental[7,8] and simulated isosteric heats of adsorption obtained from the three heterogeneous nanotube bundles (NT_Mix1, NT_Mix2, and NT_Mix3): (a, top), ethane (b, bottom) ethylene.

which was constructed using significantly larger nanotubes than those used for the other two heterogeneous bundles, are similar to the results obtained for the (10,10) and (12,12) homogeneous bundles. At low $\langle N \rangle$, q_{st} is moderate; this quantity reaches a maximum near $\langle N \rangle = 100$ (when the inner monolayer is completed). This is followed by a second, smaller, local maximum resulting from the completion of the external monolayer. Finally, there is a monotonic decrease in the isosteric heat with increasing $\langle N \rangle$.

Figure 9 a compares the simulation results for the isosteric heats obtained for ethane on the three heterogeneous bundle models with the experimental data of Rawat et al.[7] for ethane adsorbed on bundles of high-pressure carbon monoxide (HiPco) nanotubes. Excellent agreement is found for the entire coverage range. Some differences appear for the lower coverages; in this
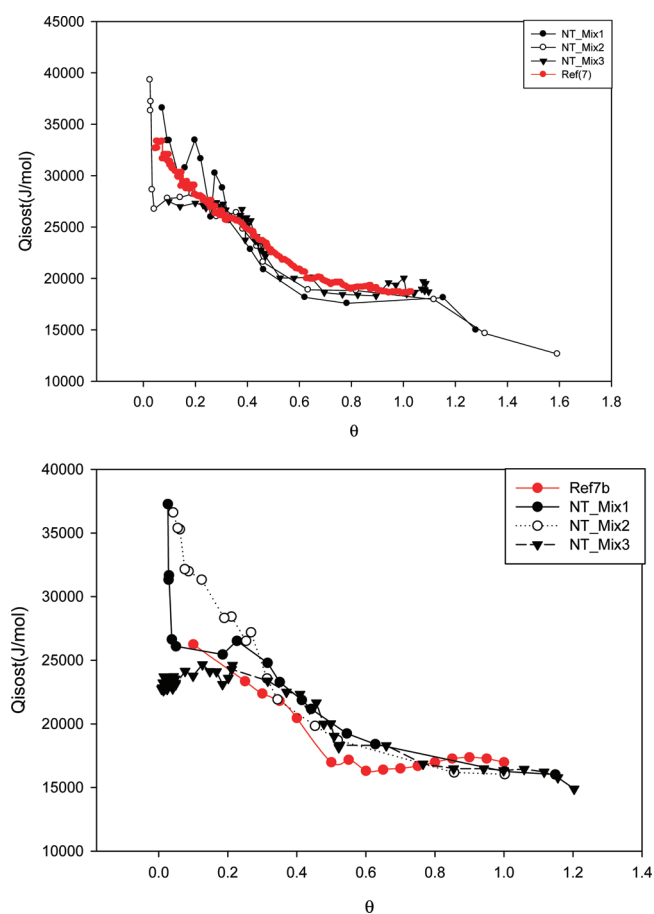
region, the three models give somewhat different results, reflecting the effect that the different diameters of the nanotubes that make up these three bundles have on the isosteric heat.

Figure 9 b presents a similar comparison between the isosteric heat values recently measured for ethylene on HiPco SWNT bundles[8] with those obtained on the three heterogeneous
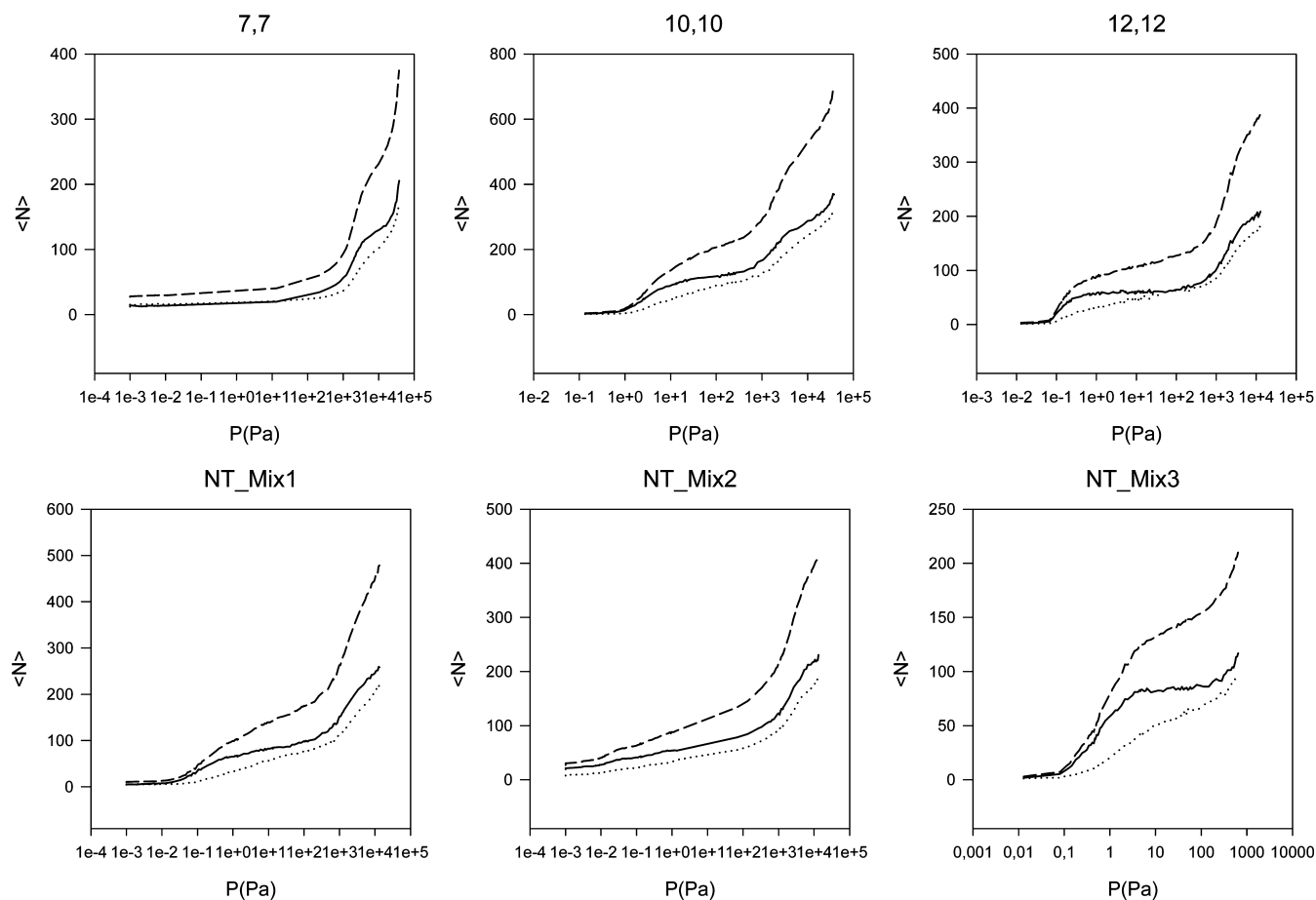
Figure 10. Simulated adsorption isotherms at 153 K for ethylene (dotted line), ethane (solid line), and the equimolar mixture (dashed line) for homogeneous (upper panels) and heterogeneous (lower panels) nanotube bundles.
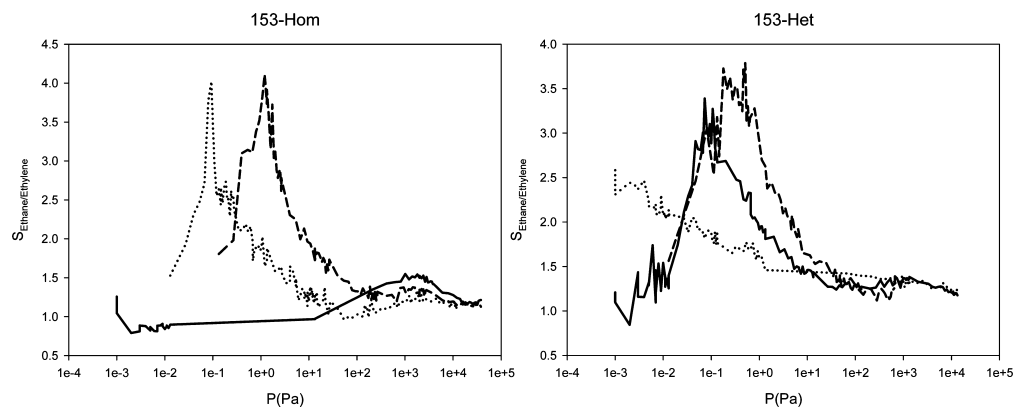

Figure 11. Separation as a function of the pressure curves at 153 K: (left) (7,7), (10,10), and (12,12) homogeneous nanotube bundles (solid, dotted, and dashed lines, respectively), (right) NT_Mix1, NT_Mix2, and NT_Mix3 heterogeneous nanotube bundles (solid, dotted, and dashed lines, respectively).

models that we have used in the simulations. As was the case for ethane, the simulations are in very good agreement with the experimental data, except at the lowest coverages where the three heterogeneous models differ.

Equimolar Mixtures. Figure 10 shows adsorption isotherms for equimolar mixtures of ethane and ethylene at T = 153 K on the three homogeneous bundles and the three heterogeneous bundles that we have used for our single-component simulations. As was the case for the single-component isotherms, more ethane than ethylene adsorbs on the bundles in

all cases at the same value of pressure (this is especially true at low pressures). As the total pressure increases, the differences between the amounts adsorbed for the two species tend to decrease.

The selectivity of different bundles was investigated with the ethylene/ethane equimolar mixture. In Figure 11 is plotted selectivity vs pressure. For homogeneous nanotube bundles, at T = 153 K, the selectivity is greater for the interior sites of the (10,10) and (12,12) nanotubes. The (7,7) nanotubes do not yield a significant degree of separation of these two species.
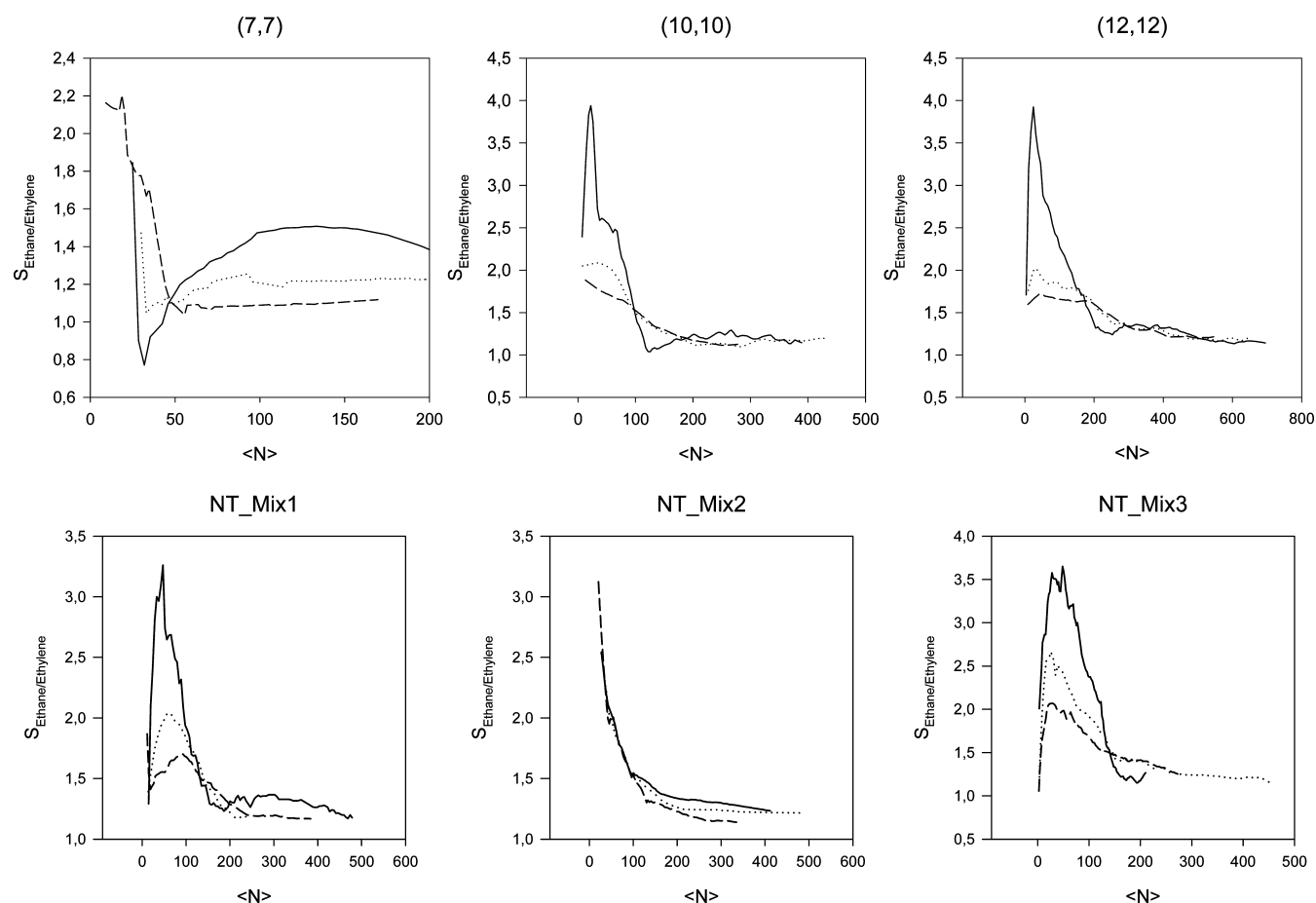
Figure 12. Selectivity as a function of coverage at 153, 273, and 343 K (solid, dotted, and dashed lines, respectively) corresponding to (7,7), (10,10) and, (12,12) homogeneous nanotube bundles (upper panels) and NT_Mix1, NT_Mix2, and NT_Mix3 heterogeneous nanotube bundles (lower panels).

In Figure 12 is plotted selectivity vs coverage. The decrease in separation ability that occurs with increasing total coverage results from the fact that, once the inner monolayer is completed, more ethylene than ethane adsorbs. Two different phenomena come into play; there is selective adsorption of ethane at low $\langle N \rangle$ as a result of attractive energy differences, and as the pressure and the loading increase, there is an increasingly higher influence of entropic effects, which favors ethylene adsorption due to its smaller size. These entropic effects result in a displacement phenomenon that occurs mainly on the internal sites. The displacement of ethane by ethylene that is observed in the larger diameter nanotubes is not present for the (7,7) homogeneous nanotube bundles. This can be explained by considering the different curvatures of the tubes. Specifically, the smaller diameter of the (7,7) nanotubes produces an adsorbed phase with lower density; the influence of entropic factors is smaller under these conditions, and consequently, the displacement of ethane by ethylene does not take place.

For the homogeneous bundles, the maximum selectivity ($S \approx 4$) occurs for the larger diameter nanotubes. However, this maximum value is reached at different pressures for different diameter nanotubes, and in each case it spans only a narrow pressure interval, as can be seen in Figure 11, left. One can speculate that for a bundle consisting of both (10,10) and (12,12) nanotubes the pressure range over which the selectivity maximum occurs would be wider than the pressure range

observed for either of the homogeneous bundles. Figure 11, right, confirms that this is the case. It shows how the pressure range over which large selectivities are attained increases when heterogeneous bundles are used.

The contribution of the external surface sites of the bundles to the selectivity is negligible. This underscores the importance of basic research aimed at developing suitable, effective activation processes for SWNT bundles if they are to be used for olefin/paraffin separation applications.

The effect of increasing temperature on the selectivity can be readily seen in Figure 12. An increase in temperature causes the selectivity to decrease for all the bundles studied. For $T = 273$ K, the maximum selectivity is $S \approx 2.0$ on all bundles (except for the NT_Mix3 bundle, which shows a slightly higher value). This value is about half of the maximum selectivity value found at 153 K.

The decrease in selectivity with increasing temperature can be understood as follows: At higher temperatures, the entropic contributions become more important and thus the number of ethylene molecules inside the nanotubes increases. This, in turn, results in a smaller selectivity.

The isosteric heat profiles calculated for each species in the ethylene/ethane mixtures on the various bundles (not shown in the figures) do not differ significantly from values obtained for the single-component gases on the same bundles at the same temperatures.

CONCLUSIONS

We have carried out Monte Carlo simulations for the adsorption of ethane and ethylene, both as single-component adsorbates and as an equimolar mixture, on several sets of homogeneous and heterogeneous nanotube bundles. The single-component results reveal the preferential adsorption of ethane over the entire pressure and temperature ranges explored. For (10,10) nanotubes ($d \approx 13.6$ Å), the density of ethane adsorbed inside the nanotubes varies only slightly over the entire temperature interval studied (even above the critical point). This is evident in the density profiles obtained in the simulations and also in the lack of variation of the isosteric heat with temperature for this bundle. Simulations performed for ethylene do not show these features.

Comparing the simulations with single-component experiments measuring the loading dependence of the isosteric heat, we find better agreement between the experimental data and the simulations on the heterogeneous bundles.

From simulations performed using equimolar mixtures, we have established that the pressure at which the bundles exhibit maximum selectivity is highly dependent on the diameter of the nanotubes used to assemble the bundles. A maximum selectivity of $S \approx 4$ was obtained at 153 K with large-diameter nanotubes. Through density profile plots, it was possible to establish that most of the adsorption selectivity was due to adsorption on the internal sites. The contribution of the external surface sites to the selectivity is negligible. In light of these findings, it seems obvious to stress the importance of the developing efficient methods for the activation of SWNTs. The selectivity was found to decrease with increasing temperature. This temperature dependence can be understood by considering the relative importance of energetic versus entropic factors in adsorption equilibrium. An increase in temperature causes the relative number of ethylene molecules inside the nanotubes to increase and therefore results in a less efficient separation.

AUTHOR INFORMATION

Corresponding Author

*E-mail: albesa@inifta.unlp.edu.ar.

ACKNOWLEDGMENTS

REFERENCES

(1) Anson, A.; Wang, Y.; Lin, C. C. H.; Kuznicki, T. M.; Kuznicki, S. M. *Chem. Eng. Sci.* **2008**, *63*, 4171.

(2) Fuertes, A. B.; Menendez, I. *Sep. Purif. Technol.* **2002**, *28*, 29.

(3) Eldrige, J. *Ind. Eng. Chem. Res.* **1993**, *32*, 2208.

(4) Anson, A.; Lin, C. C. H.; Kuznicki, T. M.; Kuznicki, S. M. *Chem. Eng. Sci.* **2010**, *65*, 807.

(5) Herdes, C.; Valente, A.; Lin, Z.; Rocha, J.; Coutinho, J. A. P.; Median, F; Vega, L. F. *Langmuir* **2007**, *23*, 7299.

(6) Kroon, M. C.; Vega, L. F. *Langmuir* **2009**, *25*, 2148.

(7) Rawat, D. S.; Migone, A. D. *Phys. Rev. B* **2007**, *75*, 195440.

(8) Rawat, D. S.; Migone, A. D. *Adsorpt. Sci. Technol.* **2011**, in press.

(9) Jiang, J.; Sandler, S. I.; Schenk, M.; Smit, B. *Phys. Rev. B* **2005**, *72*, 045447.

(10) Cruz, F. J. A.; Mota, J.P:B. *Phys. Rev. B* **2009**, *79*, 165426.

(11) Kondratyuk, P.; Wang, Y.; Johnson, J. K.; Yates, J. T. Jr. *J. Phys. Chem. B* **2005**, *109*, 20999.

(12) Cascarini, L. E.; Albesa, A. G.; Llanos, J. L.; Fertitta, A. E.; Flores, E. S. *ALDEQ* **2008**, *24*, 1.

(13) Shi, W.; Johnson, J. K. *Phys. Rev. Lett.* **2003**, *91*, 015504.

(14) LaBrosse, M. R.; Johnson, J. K. *J. Phys. Chem. C* **2010**, *114*, 7602.

(15) Esteves, I. A. C.; Cruz, F. J. A.; Muller, E. A.; Agnihotri, S.; Mota, J. P. B. *Carbon* **2009**, *47*, 948.

(16) LaBrosse, M. R.; Shi, W; Johnson, J. K. *Langmuir* **2008**, *25*, 9430.

(17) Albesa, A. G.; Fertitta, E. A.; Vicente, J. L. *Langmuir* **2010**, *26*, 786.

(18) Martin, M. G.; Siepmann, J. I. *J. Phys. Chem. B* **1998**, *102*, 2569.

(19) Wick, C. D.; Martin, M. G.; Siepmann, J. I. *J. Phys. Chem B* **2000**, *104*, 8008.

(20) Hartzog, D. G.; Sircar, S. *Adsorption* **1995**, *1*, 133.

(21) Siperstein, F.; Gorte, R.; Myers, A. L. *Langmuir* **1999**, *15*, 1570.

(22) Albesa, A. G.; Llanos, J. L.; Vicente, J. L. *Langmuir* **2008**, *24*, 3836.